UCSF

UC San Francisco Previously Published Works

Title

Identification of prostate cancer using multiparametric MR imaging characteristics of prostate tissues referenced to whole mount histopathology

Permalink

https://escholarship.org/uc/item/7cj4p5b3

Authors

Gibbons, Matthew
Starobinets, Olga
Simko, Jeffry P
et al.

Publication Date

2022

DOI

10.1016/j.mri.2021.10.008

Peer reviewed

eScholarship.org Powered by the California Digital Library
University of California

Author Manuscript

Author Manuscript

Author Manuscript

Author Manuscript

HHS Public Access

Author manuscript

Magn Reson Imaging. Author manuscript; available in PMC 2023 February 15.

Published in final edited form as:

Magn Reson Imaging. 2022 January ; 85: 251–261. doi:10.1016/j.mri.2021.10.008.

Identification of Prostate Cancer using Multiparametric MR Imaging Characteristics of Prostate Tissues Referenced to Whole Mount Histopathology

Matthew Gibbons[a], **Olga Starobinets**[a], **Jeffry P. Simko**[b,c], **John Kurhanewicz**[a,b], **Peter R Carroll**[b], **Susan M Noworolski**[a]

[a]Deparment of Radiology and Biomedical Imaging, University of California, San Francisco, 185 Berry Street, San Francisco, CA, USA

[b]Department of Urology, University of California, San Francisco, 550 16th Street, San Francisco, CA, USA

[c]Department of Pathology, University of California, San Francisco, 1825 4th Street, San Francisco, CA, USA

Abstract

In this study, the objective was to characterize the MR signatures of the various benign prostate tissues and to differentiate them from cancer. Data was from seventy prostate cancer patients who underwent multiparametric MRI (mpMRI) and subsequent prostatectomy. The scans included T2-weighted imaging (T2W), diffusion weighted imaging, dynamic contrast-enhanced MRI (DCE MRI), and MR spectroscopic imaging. Histopathology tissue information was translated to MRI images. The mpMRI parameters were characterized separately per zone and by tissue type. The tissues were ordered according to trends in tissue parameter means. The peripheral zone tissue order was cystic atrophy, high grade prostatic intraepithelial neoplasia (HGPIN), normal, atrophy, inflammation, and cancer. Decreasing values for tissue order were exhibited by ADC (1.8 10^{-3} mm^2/sec to 1.2 $10^{-3}$$mm^2$/sec) and T2W intensity (3447 to 2576). Increasing values occurred for DCE MRI peak (143% to 157%), DCE MRI slope (101%/min to 169%/min), fractional anisotropy (FA) (0.16 to 0.19), choline (7.2 to 12.2), and choline / (creatine + citrate) (0.3 to 0.9). The transition zone tissue order was cystic atrophy, mixed benign prostatic hyperplasia (BPH), normal, atrophy, inflammation, stroma, anterior fibromuscular stroma, and cancer. Decreasing values occurred for ADC (1.6 10^{-3} mm^2/sec to 1.1 $10^{-3}$$mm^2$/sec) and T2W intensity (2863 to 2001). Increasing values occurred for DCE MRI peak (143% to 150%), DCE MRI slope (101%/min to

matthew.gibbons@ucsf.edu .

Author Statement:

Matthew Gibbons: Conceptualization, Methodology, Software, Formal Analysis, Writing – Original draft preparation. **Olga Starobinets:** Methodology, Software, Investigation. **Jeffry P. Simko:** Methodology, Investigation, Writing – Reviewing and editing. **John Kurhanewicz:** Resources, Writing – Reviewing and editing. **Peter R. Carroll:** Resources, Writing – Reviewing and editing. **Susan M. Noworolski:** Conceptualization, Methodology, Investigation, Supervision, Writing – Reviewing and editing, Software, Funding acquisition.

Publisher's Disclaimer: This is a PDF file of an unedited manuscript that has been accepted for publication. As a service to our customers we are providing this early version of the manuscript. The manuscript will undergo copyediting, typesetting, and review of the resulting proof before it is published in its final form. Please note that during the production process errors may be discovered which could affect the content, and all legal disclaimers that apply to the journal pertain.

Declaration of interest: none

Author Manuscript Author Manuscript Author Manuscript Author Manuscript

137%/min), FA (0.18 to 0.25), choline (7.9 to 11.7), and choline / (creatine + citrate) (0.2 to 0.6). Logistic regression was used to create parameter model fits to differentiate cancer from benign prostate tissues. The fits achieved AUCs ≥ 0.91. This study quantified the mpMRI characteristics of benign prostate tissues and demonstrated the capability of mpMRI to discriminate among benign as well as cancer tissues, potentially aiding future discrimination of cancer from benign confounders.

Keywords

prostate cancer; multiparametric MRI; histopathology; diffusion-weighted imaging; dynamic contrast-enhanced imaging; magnetic resonance spectroscopy imaging

1. Introduction

Prostate cancer (PCa) is extremely prevalent in men [1,2]. Nonetheless, the risk of treatment side effects is high while the risk of progression is low [3]. The amount and grade of disease are important predictors for prostate cancer progression and Gleason grade assigned to biopsy results is the standard for diagnosis [4]. However, the prostate is inadequately sampled by standard biopsy leading to under diagnosis of higher grade disease in some [5]. Biopsy is also an invasive procedure with potentially significant adverse effects [6].

Multi-parametric MRI (mpMRI) has been shown to be a powerful, non-invasive technique for detecting, locating, and determining extent of PCa [7,8,9]. With the advent of the Prostate Imaging Reporting and Data System (PI-RADS), the application of mpMRI for assessment of PCa has been standardized [10]. Accurate detection is confounded by the tremendous heterogeneity of tissues within the prostate. With the advent of advanced machine learning and artificial intelligence approaches to automate prostate cancer detection on MRI, understanding of the MR tissue characteristics of benign, normal and abnormal, tissues within the prostate is important to optimize detection accuracy. The diverse underlying anatomy and physiology of these different tissues suggests that the full range of mpMRI capability is necessary to capture potentially subtle differences among these tissues.

The MR characterization and differentiations of benign tissues may aid future radiologist and artificial intelligence approaches to separate cancers from benign confounders, ultimately aiding clinical assessment. Therefore, in this study, the objective was to characterize the MR signatures of the various benign prostate tissues and to differentiate them from cancer. In the data sets and analysis, an extensive range of benign tissue types was included, and logistic regression analysis was performed to facilitate automated differentiation of cancer.

2. Materials and Methods

2.1. Patients

Seventy men with biopsy proven prostate cancer were included in this study. The cohort was documented previously in our study of mpMRI cancer characteristics compared to

Author Manuscript Author Manuscript Author Manuscript Author Manuscript

histopathology post radical prostatectomy with eight excluded due to lack of complete MR Spectroscopic Imaging (MRSI) data [11]. The MRI scans were acquired between 2007 and 2014. Patients were excluded if MRI preceded surgery by more than one year or if they had treatment for prostate cancer (i.e. hormonal therapy) before surgery. The Institutional Review Board approved the study and the methods met Health Insurance Portability and Accountability Act compliance. Written informed consent was obtained from all patients.

2.2. MR Imaging

MR images were acquired with a 3T scanner (GE Healthcare, Chicago, IL, USA) using an external phased array coil and an expandable balloon endorectal coil (MedRad, Bayer HealthCare LLC, Whippany, NJ). Summaries of scan conditions are reported below while more complete details were provided in Starobinets, et. al [11]. The scan types included T2-weighted imaging, Diffusion weighted imaging (DWI), Dynamic Contrast Enhanced MR imaging (DCE MRI), and MR Spectroscopic Imaging (MRSI). Since the endorectal coil has a non-uniform reception profile, a correction was applied to raw images [12] to allow quantitative assessment across the field-of-view (FOV). Images used for this analysis were acquired with slices in an oblique axial plane. The anatomical T2-weighted images were obtained using a Fast Spin Echo (FSE) scan (TR/TE 6000/96ms, FOV 18 cm, slice thickness 3mm, matrix 512×512).

Diffusion weighted images (DWI) were obtained using a 2D single-shot echo-planar imaging (EPI) spin echo sequence (TR/TE 4000/78-90ms, b-value 0 and 600 s/mm^2, slice thickness 3mm). Scans were taken with either a conventional FOV (matrix 128 x 128) or reduced FOV (128 x 64) with the latter providing reduction of susceptibility artifacts [13]. Both apparent diffusion coefficient (ADC) maps and fractional anisotropy (FA) maps were generated with in-house software. ADC was calculated as [13]

$$\mathrm{ADC} = -\frac{1}{\mathrm{b}}\ln\left(\frac{\mathrm{S_{gm}}}{\mathrm{S_0}}\right) \quad [1]$$

where b is the b-value, S_{gm} is the signal intensity mean over the six gradient directions at b=600, and S_0 is the signal intensity of the image at b=0. FA was calculated from the DWI tensor eigenvalues, (λ_1, λ_2, λ_3) as [14]

$$FA = \left[\frac{3((\lambda_1 - \lambda_m)^2 + (\lambda_2 - \lambda_m)^2 + (\lambda_3 - \lambda_m)^2)}{2(\lambda_1^2 + \lambda_2^2 + \lambda_3^2)}\right] \quad [2]$$

DCE MRI was completed with a 3D fast Spoiled Gradient Recalled (SPGR) sequence (TR/TE 3.5/0.9ms, flip angle 5°, slice thickness 3mm, contrast gadopentetate dimeglumine (Gd-DTPA) (Magnevist; Bayer, Whippany, NJ), time 5 min, intervals between 6 to 13 sec). Semi-quantitative properties of contrast uptake into the prostate were tracked with maps of peak enhancement (PE), maximum enhancement slope (ES), and washout rate (WO). The maps were generated by calculating these quantities for each voxel [15] from the temporal evolution of DCE MRI images.

Author Manuscript Author Manuscript Author Manuscript Author Manuscript

More quantitative, physiological properties were derived through pharmacokinetic modeling of the DCE MRI data. Pharmacokinetic parameters and maps were created using a Luminal Water (LW) model [16] which is a modification of the Tofts-Kermode model [17]. The derived quantities were the transfer constant (K^{trans}), the fractional extravascular, extracellular volume (v_e), and the luminal water fractional volume (v_L). The LW model adds the v_L parameter under the assumption that contrast agent cannot enter water within the prostate ductal lumen.

MRS images were obtained using a 3D flyback, echo planar Point RESolved Spectroscopy Chemical Shift Imaging (PRESS CSI) scan (TR/TE=2000/85ms, matrix 16×12×10, resolution 5.4 mm zero-filled to 5.4×2.7×2.7mm^3, voxel volume 0.04cc) [18]. Peak height was measured to determine choline, creatine, and citrate levels. Additionally, choline / citrate ratios were computed.

2.3. MR Image Normalization

T2-weighted and DCE MRI images were normalized to decrease the variance from patient to patient. The scaling factor was determined by averaging over two ROIs selected within the obturator muscles next to the prostate. The normalized T2W for each ROI, *i*, for a patient, j, was given by:

$$T2W_{norm\_i} = \frac{T2W_i}{T2W_{muscle\_j}} \quad [3]$$

The DCE MRI images were scaled based on the peak enhancement, PE_{muscle}, averaged over two muscle ROIs for each case, *j*, and the average muscle enhancement over all cases. The normalization equations for DCE MRI PE, DCE MRI ES, and DCE MRI WO of each ROI, *i*, were:

$$PE_{norm\_i} = PE_i \cdot \left(\frac{PE_{muscle\_ave}}{PE_{muscle\_j}}\right) \quad [4]$$

$$ES_{norm\_i} = ES_i \cdot \left(\frac{PE_{muscle\_ave}}{PE_{muscle\_j}}\right) \quad [5]$$

$$WO_{norm\_i} = WO_i \cdot \left(\frac{PE_{muscle\_ave}}{PE_{muscle\_j}}\right) \quad [6]$$

2.4. Histopathology

The prostate specimens were prepared with neutral buffered formalin as the fixative. Similar to the MRI slices, the physical prostates were sectioned into 3 mm slices with a manual precision slicer and embedded in paraffin. The sections were prepared on slides by cutting to 4 μm thickness and staining with hematoxylin and eosin (H&E) and were characterized by the study pathologist.

Author Manuscript Author Manuscript Author Manuscript Author Manuscript

2.5. Identifying Regions of Interest

Tissues were delineated and labeled by the pathologist as separate Regions of Interest (ROI). Along with an assigned tissue label, a specific boundary was drawn around each ROI. In our previous study [11], cancerous ROIs differentiated by Gleason grade and regions of benign glandular tissue (normal and cystic atrophy) were compared. In this study additional benign tissues were identified in the peripheral zone (cystic atrophy, high grade prostatic intraepithelial neoplasia (HGPIN), atrophy, and inflammation) and the transition zone (atrophy, cystic atrophy, inflammation, mixed benign prostatic hyperplasia (BPH), stroma, and anterior fibromuscular stroma) for characterization. Cystic atrophy presents as glandular tissue with a loss of epithelial cells, but intact basement membranes, while retaining fluid in the glandular lumen [19]. Atrophy reflects loss of cytoplasm of secretory cells and hence reduced cell size [19]. In standard atrophy this results in reduced gland sizes and loss of papillary infoldings of typical benign glands, while in cystic atrophy the atrophic glands are expanded and stretched by development of cystic spaces. Inflammation presents as an infiltration of lymphocytes into the tissue with generally resultant atrophy [20]. Transition zone tissue generally comprises a mixture of normal benign glands, along with hyperplastic glands and stroma of BPH. Anterior fibromuscular stroma was stroma tissue located at the anterior edge of the prostate without the presence of any glands.

The histological ROI location information from the slides was translated to the MRI images by manually drawing MRI ROIs onto the T2W images based on anatomical landmarks, in homogeneous regions, and with consensus of two readers. Additional MRI ROIs were placed with consensus of the two readers, in unlabeled, non-urethral, homogeneous regions on MRI, and labeled as normal. The two readers were members of our prostate imaging group, with 3 and 20 years' experience reviewing prostate MRIs. Manual registration of other images (ADC, DCE, etc.) to the T2W images was performed if deemed necessary by visual inspection. To improve confidence in ROI placement, the MRI ROIs were defined smaller than the histology ROIs to avoid artifacts from motion. Only MRI ROIs larger than 0.05 cc were retained in the final data set as further protection against artifacts. Finally, ROIs were rejected if distortion from susceptibility artifacts was evident in the DWI images and ADC maps at the location of an ROI. In general susceptibility issues were confined to the rectum and PZ interface [13].

2.6. Statistical Analysis

The mpMRI parameter distributions were characterized for each tissue type and were analyzed separately for TZ and PZ to address any potential zonal differences due to the underlying tissue compositions of the two regions. The image intensities or map values were listed as mean ± standard deviation. The Tukey-Kramer honestly significant difference (HSD) [21] test was used to compare means across tissue types. Differences between means were shown by connected letters reports [21] which provide letter labels to distinguish groups of tissues with statistical significance p-values less than 0.05. Distributions such as ROI size, which were not normally distributed, were reported as median (1^{st} quartile, 3^{rd} quartile). MR characteristics were compared for tissue types that were present in both the PZ and TZ to determine any significant differences.

Author Manuscript Author Manuscript Author Manuscript Author Manuscript

Logistic regression with the MRI parameters as factors was implemented to create models for differentiating prostate cancer. JMP software (JMP, Version 14, SAS Institute Inc., Cary, NC) was used for distribution characterization and logistic regression [21]. The logistic regression analysis was preceded by a mixed, stepwise algorithm where factors were added or removed from the fit depending on their significance [21]. In this analysis the criterion for inclusion was a p-value ≤ 0.15. Once complete, the fits were manually checked for overfitting. If the fit dependency for a factor was inconsistent with the dependencies indicated by the univariate means, the factor was removed from consideration and the fit recomputed. Parameters from the same modality, such as DCE MRI, may have some correlation or be affected by the same scan artifacts. However, each parameter possessed unique information since each modality separates parameters by time (DCE MRI), frequency (MRSI), or tensor characteristics (DWI). For this reason, parameters from the same modality were all fed into in the stepwise regression control algorithm.

The receiver operating characteristic (ROC) curves and the area under the curve (AUC) were used as metrics to evaluate the logistic regression fits. Sensitivity and specificity were reported at the point on the ROC curve closest to equal sensitivity and specificity, and sensitivity - (1 - specificity) at a maximum. This weights false negatives and false positives in a similar manner although the various tissue groups were not of equal size. As with the means comparisons, the models were completed separately for the TZ and the PZ. To assess the performance of each model, a 4-fold cross-validation was performed. The AUC mean and 95% confidence interval were calculated.

3. Results

The demographics of the patients were as follows: mean age 64.1±6.1 years, median PSA 6.2 ng/ml (Q1=4.3 ng/ml, Q3=8.8 ng/ml), median prostatectomy Gleason score 7 (Q1=6, Q3=8). Given the inclusion criteria, the median time between MRI scan and prostatectomy was 38 days (Q1=14 days, Q3=76.8 days). Additional patient information can be found in Starobinets, et. al [11].

Table 1 is a summary of ROI counts and sizes for the tissue types. In total there were 617 ROIs in the TZ and 811 ROIs in the PZ. The sizes are the ROI volumes within each 3mm MRI slice. The median volumes were similar in the TZ (0.12cc) and the PZ (0.11cc), albeit with wide ranges (0.02cc to 0.88cc in the TZ and 0.2cc to 1.46cc in the PZ).

A set of mpMR images and corresponding histopathological slide from a case are shown in Figure 1. The tissue types demonstrate different combinations of hyper- and hypo-intensities in the different MR images. The region of cancer exhibits low T2W, low ADC, and low DCE MRI washout while having high DCE MRI slope. The AFMS exhibits hyperintense fractional anisotropy with hypointense T2W and ADC. The cystic atrophy exhibits hyperintense T2W and ADC.

The means of the T2W and DCE PE distributions after normalization were T2W (2.6) and DCE PE (43%). The coefficients of variation (COV) before and after normalization were

Author Manuscript Author Manuscript Author Manuscript Author Manuscript

T2W (0.32 → 0.24) and DCE PE (0.33 → 0.26) with p-values from two sided F-tests of 0.009 and 0.033 respectively.

The imaging parameters for tissues in the PZ are compared in the box plots of Figure 2. The tissues were ordered according to general trends in the means of the tissues as: cystic atrophy, High Grade PIN, normal PZ, atrophy, inflammation, and cancer PZ. Connected letter reports within each plot highlight the trends by indicating differences for p-value < 0.05 with different letter labels. The means and standard deviations of the parameters are reported in Table 2. The parameters with decreasing values for the given tissue order from cystic atrophy to cancer were ADC (from 1.8 to 1.2 $10^{-3}mm^2/sec$) and T2-weighted normalized intensity (from ~ 3.3 to 2.5). The parameters with generally increasing values were DCE MRI PE (from 43 to 57 %), DCE MRI ES (from 101 to 169 %/min), and choline / citrate (0.3 to 0.9), with the notable exception that HGPIN had higher DCE MRI ES, faster DCE MRI WO, shorter peak time, higher K^{trans}, lower v_L, and higher choline than all the other benign tissues.

The imaging parameters for tissues in the TZ are compared in the box plots of Figure 3. The tissues were ordered according to general trends in the means of the tissues as: cystic atrophy, mixed BPH, normal TZ, atrophy, inflammation, stroma, AFMS, and cancer TZ. Connected letter reports within each plot highlight the trends by indicating differences for p-value < 0.05, similar to Figure 2. The means and standard deviations of the parameters are reported in Table 3. The parameters with generally decreasing values for the given tissue order from cystic atrophy to cancer (excluding stroma and AFMS) were ADC (from 1.6 to 1.1 $10^{-3}mm^2/sec$) and T2-weighted normalized intensity (2.7 to 1.9). The parameters with generally increasing values were DCE MRI PE (43 to 50 %), DCE MRI slope (101 to 137 %/min), FA (0.18 to 0.25), choline (7.9 to 11.7), and choline / citrate (0.3 to 0.7).

The tissues which were identified in both the PZ and TZ (normal, cystic atrophy, atrophy, and inflammation) are compared in Table 4. Listed are the ratio of PZ versus TZ parameters and p-value from the mean comparison of the distributions. DCE MRI WO is listed as a difference rather than a ratio since washout can be either positive or negative. Only those parameters with p-value < 0.05 for two or more of the tissues are included.

The ROC curves for the logistic regression analysis were plotted in Figure 4 with AUC of 0.91 and 0.93 for the PZ and TZ respectively. Figure 5 is a profiler plot of the logistic regression results which show the trends in probability of PCa versus the mpMRI factors. Figures 5 and 6 are profiler plots of the logistic regression results which show the trends in probability of PCa versus the mpMRI factors. Figure 5 illustrates the trends for the TZ model with cursors set for parameters between PCa and benign. Figure 6 has a comparison in the PZ between PCa, inflammation, and cystic atrophy. The 4-fold cross validation results are listed in Table 5 with the mean and 95% CI for the models in the PZ and TZ.

4. Discussion

As evidenced by the statistically significant differences in the parameter means comparisons and the high AUC resulting from the logistic regression fits, this study was able to enhance

Author Manuscript Author Manuscript Author Manuscript Author Manuscript

discrimination of PCa from multiple prostate tissue types simultaneously. The 4-fold cross validation of the fits exhibited acceptable variance in the distributions of the ROC AUC. The mean AUCs of the validation fits were all greater than 0.90 and were within 0.01 of the AUCs for the fits which utilized all data.

The use of 2nd order fits improved the results by a) allowing steeper transitions between probabilities and b) allowing non-monotonic parameter dependencies of probabilities. This quantitative procedure may mitigate errors inherent in PCa identification where the distributions of MRI parameters have large overlap [22,23]. This benefit is evident in the parameters of DCE PE, FA, T2W, and v_e where TZ PCa has intermediate values, with labels highlighted in yellow (Fig 3c, g, i). An example of the beneficial effect on the cancer probability model for the TZ is shown in Figure 5. Despite the total benign distributions encompassing the PCa distributions, individual benign tissues did exhibit separation from PCa. In this example, the lower T2W and higher FA of AFMS versus PCa results in a peak in cancer probability for those parameters. So, having the benign tissues separated by type allows PCa to be distinguished by these parameters. Thus, more parameters can contribute to the logistic regression fits, increasing the ROC AUC.

The utility of multiple parameters is shown in the profiler plots of Figure 6 for three tissue types in the PZ (PCa, inflammation, and cystic atrophy). Each tissue type is represented with parameters set at the mean for the tissue type. While inflammation is not exceptionally different than PCa for T2W; a combination of parameters ADC, DCE ES, DCE WO, and choline / citrate contribute to a large difference in probability of cancer (0.82 vs 0.26). Cystic atrophy, with a larger difference in ADC from PCa, has a lower probability of cancer of 0.05. The improved ROC AUC is achieved despite errors (image artifacts, noise, or tissue variability) existing in the individual scans for each patient.

In PZ cancerous tissue, the prostatic glands become smaller and irregular with breakdown of the basement membranes [2]. There is the potential for more cell and blood vessel growth [2]. Consistent with more densely packed tissue, both ADC and T2 were hypointense [24]. The Fractional Anisotropy for cancer had a value intermediate between stroma and other benign tissues. The 2nd order fit captured the non-linear response. As glands with their fluid-filled spaces would have inherently low fractional anisotropy, the loss of the glands in cancer as the glands are replaced by cells naturally leads to higher fractional anisotropy. Li, et al. [25], who found higher FA with higher Gleason score cancers, have conjectured that increased FA in cancer relative to normal tissue may be due to increased concentration of cells. The present results also indicate that directionality in stroma, particularly AFMS, is larger than all other tissues. With the assumption that Gd-DTPA cannot penetrate the basement membrane of intact glands [26], the breakdown of the basement membrane leads to more space for the contrast agent to accumulate, decreasing v_L, increasing v_e and PE and indirectly increasing slope, washout and K^{trans}. Consistent with this, DCE MRI parameters were as expected, having higher slope and shorter time to peak (faster uptake) combined with faster washout [27]. The higher K^{trans} may also reflect increased and/or potentially leaky blood vessels [2]. MRSI exhibited increased choline (cellular proliferation) and decreased citrate (loss of normal epithelial layer function and glandular spaces) [2,28].

Author Manuscript Author Manuscript Author Manuscript Author Manuscript

The PZ had fewer significant factors than the TZ with ADC dominating, resulting in a slightly lower AUC.

The benign tissues had mpMRI characteristics consistent with their biological properties. Anterior fibromuscular stroma (AFMS) stood out with high FA which is expected for the anisotropic, muscular fiber structure of tissue [29]. As compared to the other benign tissues, the hypointense ADC and T2W, low DCE MRI slope, and absence of washout, are consistent with the non-glandular, dense structure of the AFMS with its lower perfusion than other tissues [30]. All spectroscopy quantities were low for the non-glandular AFMS. The PK parameters were not reported since the luminal water model is not appropriate for such tissue lacking glands [16].

Stroma in the TZ had FA higher than the other tissues but not as high as the AFMS, consistent with the relatively ordered stromal cells as opposed to glandular tissues. Differentiating from the other benign tissues, TZ stroma had higher DCE MRI peak, absence of DCE MRI washout, high v_e, and low v_L consistent with a lack of basement-membrane-intact glands, leading to more space for the contrast agent to accumulate [26]. Unlike AFMS, the TZ stroma did exhibit a choline signal on the higher end for benign tissues while it also had low citrate. These are again consistent with its lack of glands and associated, citrate-producing epithelial cells, and thus, higher cellular concentration and lower citrate [31].

The remaining tissues in the TZ had characteristics differentiating between a group (1) inflammation and atrophy; and a group (2) cystic atrophy and mixed BPH. The MRI parameters for normal tissue tended to have values toward the center of the range between the two groups. ADC, T2W, creatine, and citrate are larger in group (2). V_e and FA are smaller in group (2). These trends in MR characteristics are generally consistent with more water, larger glands, and less stroma in group (2) than group (1) [19,32]. Atrophy presents as a loss of epithelial cells, and a resultant loss of glandular lumen. Inflammation presents as lymphocytes infiltrating the tissue which generally also becomes atrophic. As the lymphocytes infiltrating tissue represented only 5 - 20% of the tissue in our study, it is not surprising that atrophy and inflammation (with its generally co-existing atrophy) could not be statistically separated with the MR parameters in this study. One notable difference between group (2) tissues is in the luminal water fraction, v_L. The cystic atrophy mean was 0.29, and mBPH mean was 0.17 while the group 1 tissues had v_L mean ~ 0.2. The v_L parameter appeared to be reflective of the enlarged, intact glandular lumen in cystic atrophy [19].

Tissue types in the PZ were differentiated between groups (1) inflammation and atrophy; and (2) cystic atrophy and HGPIN. The trends for the PZ are similar to those noted above for the TZ. Finally, between cystic atrophy and HGPIN, there were significant differences ($p < 0.05$) in the DCE MRI and PK parameters. The enhancement slope, washout, peak time, K^{trans} of cystic atrophy were closer to the group (1) tissues than to HGPIN. ADC and T2W of HGPIN were similar to the group (1) tissues. The DCE MRI and PK parameters suggest that the perfusion is higher for HGPIN than other glandular tissues and that there is less intact glandular structure (lower v_L), similar to cancer. These results are consistent with

Author Manuscript Author Manuscript Author Manuscript Author Manuscript

HGPIN having glandular and ductal architecture near normal with increases in intraductal epithelial cells [2,33].

Overall, abnormal benign tissues were prevalent in this cohort. Based on the ROIs with sufficient size and conspicuity to be correlated to MRI (Table 1), 80% of patients had cystic atrophy and 83% had atrophy and inflammation in the PZ, demonstrating that these tissues are important contributors to the MRI intensities observed in the prostate.

The AUC of our fits, 0.91 for peripheral zone and 0.93 for transition zone, are favorable relative to literature values ranging from 0.74 to 0.96 [22,34,35,36] for the peripheral zone and 0.68 to 0.92 [22,37,38,39] for the transition zone. Several features of this study improve the robustness of the model fits. The analysis takes advantage of many MRI parameters versus few [22,40,41], whole mount histology versus biopsy [37], and many ROIs per patient instead of patient means or single VOIs [35,36]. The use of many tissues and ROIs increases the variance of tissue characteristics causing a greater challenge for modeling. However, the separation of tissues improves the ability to differentiate cancer because divergent mpMRI trends among benign tissues are accessible to the fitting. The resulting analysis provides a different and more comprehensive perspective for the entire prostate than articles comparing individual tissues (normal [9,34,35], BPH [42,43], HGPIN [44], and inflammation [45]) to PCa. In Litgens, et. al. [46,47], a cascading classifier method was used to sequentially discriminate inflammation, HGPIN, BPH, atrophy, and finally cancer. This study achieved an accuracy of 0.76 using parameters from T2W, DWI, and DCE MRI. While the classification algorithm and the order for extracting PCa from other tissues are different from our method, the utility of identifying multiple tissues and using multiple parameters is evident.

The PZ versus TZ comparison in table 5 has values that indicate higher free water content in the PZ (higher ADC, T2W, vL and lower FA). The PZ had lower creatine than the TZ representing lower cell density. This is consistent with the higher glandular structure in the PZ. The slower DCE MRI washout implies a higher intact luminal water space, resulting in a slower washout in such tissues [16].

This study has several limitations. The manual method of ROI definition and alignment has limitations as noted previously [11], such as bias in localizing tissues. Impact from distortion in DWI derived maps is possible which could affect properties within ROIs and alignment of ROIs with the T2W image. Korn, et. al. [13] performed quantitative distortion analysis of a cohort that included scans from this study. As noted in the methods section 2.5, DWI distortion in the current study was addressed by defining ROIs in homogeneous regions and not including ROIs where significant distortion existed. Problematic distortion sufficient for rejection of ROIs existed in 15 of the 70 cases. Since the distortion was generally only in the PZ near the rectum, rejected ROIs were less than 10% of the total. With these precautions, distortion may contribute to the variance in the ADC and FA distributions but have minimal impact on the means.

While the information reported in this study is a necessary baseline, accuracy in the detection of PCa could be reduced by DWI distortion. Both manual assessment by

Author Manuscript Author Manuscript Author Manuscript Author Manuscript

radiologists and automated methods will be affected. Error would be partially mitigated by inclusion of the other mpMRI factors (T2W, DCE, and MRSI) as indicated by the high ROC AUCs of the PZ and TZ models. Nonetheless given the importance of DWI dependent images as biomarkers for PCa, distortion to DW images and its reduction has been the subject of many recent studies. Giganti et al [48] summarized studies for improving MR imaging in four areas: MRI sequences, MRI hardware, patient preparation, and adherence to technical standards. In addition to understanding the baseline MRI characteristics of prostate tissues, implementation of image improvements will help to enable quantitative, automated procedures for detecting PCa.

In this study, all ROIs were analyzed as separate data instances and not combined into connected lesions. This preserved the slice-to-slice variation across a lesion. Since not all tissues were identified in every patient, the data set does not capture the total distribution caused by scan and patient variability. The tissues most affected by this limitation were stroma and cTZ. Adding more patients to the cohort would reduce uncertainty in this result. Skew in the distributions and errors in the means could also be affected by unequal ROI sample sizes and ROI volumes for the different tissue types. However, excluding the stroma tissues, the median ROI volumes were within a factor of two across the tissue types. The comparison between non-cancer and cancerous tissues was improved by including all benign tissues with significant numbers of ROIs in the analysis. Of particular note, the number of ROIs for normal PZ and TZ were low in this study, in part due to the predominance of benign abnormalities and in part due to methodology of defining “normal” for this study.

As the collection of heterogeneous benign tissues can present with a wide range of MR parameter values, separating and characterizing the individual benign tissues allows their separate patterns to be elucidated and used to improve the detection of cancer. This can be through better discrimination of cancer from a benign confounder and by the use of more complex, multivariate models to separate cancer from benign tissues.

5. Conclusion

This study summarized the mpMRI characteristics of cancer and of benign prostatic tissues (AFMS, stroma, normal, inflammation, atrophy, HGPIN, mixed BPH, and cystic atrophy). It also demonstrated the capability of mpMRI to distinguish cancer from the various benign tissues in the prostate. This characterization of the MR signatures of the prostate may aid future qualitative and quantitative detection of prostate cancer, improving discrimination versus benign confounders.

Funding sources

This work was supported by the National Institutes of Health [grant number R01 CA148708] and the California Tobacco-Related Disease Research [grant number 28IR-0060].

Abbreviations:

ADC	apparent diffusion coefficient
AUC	area under the receiver operating characteristics curve

Author Manuscript Author Manuscript Author Manuscript Author Manuscript

DCE MRI	dynamic contrast-enhanced magnetic resonance imaging
DCE PE	dynamic contrast-enhanced peak enhancement
DCE ES	dynamic contrast-enhanced enhancement slope
DCE WO	dynamic contrast-enhanced washout slope
DWI	diffusion weighted imaging
GS	Gleason Score
$\mathbf{K^{trans}}$	volume transfer constant
LR	logistic regression
MP	multiparametric
MRSI	magnetic resonance spectroscopic imaging
PCa	prostate cancer
PZ	peripheral zone
ROI	region of interest
TZ	transition zone
$\mathbf{v_e}$	fractional extravascular, extracellular volume
$\mathbf{v_L}$	fractional luminal volume

References

[1]. Siegel RL, Miller KD, Jemal A. Cancer statistics, 2016. CA. 2016;66(1):7–30. [PubMed: 26742998]

[2]. Rosenkrantz AB. MRI of the prostate: a practical approach. New York: Thieme Medical Publishers, Inc. 2017.

[3]. Resnick MJ, Koyama T, Fan KH, et al. Long-term functional outcomes after treatment for localized prostate cancer. N Engl J Med. 2013;368(5):436–445. doi:10.1056/NEJMoa1209978. [PubMed: 23363497]

[4]. Epstein JI, Partin AW, Sauvageot J, Walsh PC. Prediction of progression following radical prostatectomy. A multivariate analysis of 721 men with long-term follow-up. Am J Surg Pathol. 1996;20(3):286–292. doi:10.1097/00000478-199603000-00004 [PubMed: 8772781]

[5]. Serefoglu EC, Altinova S, Ugras NS, et al. How reliable is 12-core prostate biopsy procedure in the detection of prostate cancer? Cuaj-Can Urol Assoc. 2013;7(5-6):E293–E298. doi:10.5489/cuaj.11224.

[6]. Loeb S, Vellekoop A, Ahmed HU, et al. Systematic review of complications of prostate biopsy. Eur Urol. 2013;64(6):876–892. doi:10.1016/j.eururo.2013.05.049. [PubMed: 23787356]

[7]. Hoeks CM, Barentsz JO, Hambrock T, et al. Prostate cancer: multiparametric MR imaging for detection, localization, and staging. Radiology. 2011;261(1):46–66. doi:10.1148/radiol.11091822. [PubMed: 21931141]

[8]. Johnson LM, Turkbey B, Figg WD, Choyke PL. Multiparametric MRI in prostate cancer management. Nat Rev Clin Oncol. 2014;11(6):346–353. doi:10.1038/nrclinonc.2014.69. [PubMed: 24840072]

Author Manuscript Author Manuscript Author Manuscript Author Manuscript

[9]. Starobinets O, Korn N, Iqbal S, Noworolski SM, Zagoria R, Kurhanewicz J, Westphalen AC. Practical aspects of prostate MRI: hardware and software considerations, protocols, and patient preparation. Abdom Radiol. 2015;4(5):817–30. doi:10.1007/s00261-015-0590-x.

[10]. ACR (2019) MR Prostate Imaging Reporting and Data System version 2.1. American College of Radiology. https://www.acr.org/-/media/ACR/Files/RADS/Pi-RADS/PIRADS-V2-1.pdf.

[11]. Starobinets O, Simko JP, Kuchinsky K, Kornak J, Carroll PR, Greene KL, Kurhanewicz J, Noworolski SM. Characterization and stratification of prostate lesions based on comprehensive multiparametric MRI using detailed wholemount histopathology as a reference standard. NMR Biomed. 2017;30(12):e3796. doi:10.1002/nbm.3796.

[12]. Noworolski SM, Reed GD, Kurhanewicz J, Vigneron DB. Post-processing correction of the endorectal coil reception effects in MR spectroscopic imaging of the prostate. J Mag Reson Imaging. 2010;32(3):654–662. doi:10.1002/jmri.22258.

[13]. Korn N, Kurhanewicz J, Banerjee S, et al. Reduced-FOV excitation decreases susceptibility artifact in diffusion-weighted MRI with endorectal coil for prostate cancer detection. Magn Reson Imaging. 2015;33(1):56–62. doi:10.1016/j.mri.2014.08.040. [PubMed: 25200645]

[14]. Basser PJ, Pierpaoli C. Microstructural and physiological features of tissues elucidated by quantitative-diffusion-tensor MRI. 1996. J Magn Reson. 1996;111:209–219. doi:10.106/jmre.1996.0086.

[15]. Noworolski SM, Henry RG, Vigneron DB, Kurhanewicz J. Dynamic contrast-enhanced MRI in normal and abnormal prostate tissues as defined by biopsy, MRI, and 3D MRSI. Magn Reson Med. 2005;53(2):249–255. doi:10.1002/mrm.20374. [PubMed: 15678552]

[16]. Noworolski SM, Reed GD, Kurhanewicz J. A Novel Luminal Water Model for DCE MRI of Prostatic Tissues. Paper presented at: International Society for Magnetic Resonance in Medicine 2011; Montreal.

[17]. Tofts PS, Kermode AG. Measurement of the blood-brain barrier permeability and leakage space using dynamic MR imaging. 1. Fundamental concepts. Magn Reson Med. 1991;17(2):357–367. doi:10.1002/mrm.1910170208. [PubMed: 2062210]

[18]. Chen AP, Cunningham CH, Ozturk-Isik E, et al. High-speed 3T MR spectroscopic imaging of prostate with flyback echo-planar encoding. J Magn Reson Imaging. 2007;25(6):1288–1292. doi:10.1002/jmri.20916. [PubMed: 17520729]

[19]. Tomas D, Kruslin B, Rogatsch H, Schafer G, Belicza M, Mikuz G. Different Types of Atrophy in the Prostate With and Without Adenocarcinoma. Eur Urol. 2007;51:98–104. doi:10.1016/j.eururo.2006.06.001. [PubMed: 16824675]

[20]. Murtola, et al. Inflammation in benign prostate tissue and prostate cancer in the finasteride arm of the Prostate Cancer Prevention Trial. Cancer Epidemiol Biomarkers Prev. 2016;25(3):463–469. doi:10.1158/1055-9965.EPI-15-0987. [PubMed: 26715424]

[21]. JMP® 14 Fitting Linear Models. Cary, NC: SAS Institute Inc. 2018. ISBN 978-1-63526-512-5.

[22]. Dikaios N, Giganti F, Sidhu HS et al. Multi-parametric MRI zone-specific diagnostic model performance compared with experienced radiologists for detection of prostate cancer. Eur Radiol. 2019;29:4150–4159. doi:10.1007/s00330-018-5799-y. [PubMed: 30456585]

[23]. Rosenkrantz AB, Taneja SS. Radiologist, Be Aware: Ten Pitfalls That Confound the Interpretation of Multiparametric Prostate MRI. AJR Am J Roentgenol. 2014;202:109–120. doi:10.2214/AJR.13.10699. [PubMed: 24370135]

[24]. Hambrock T, Somford DM, Huisman HJ, et al. Relationship between Apparent Diffusion Coefficients at 3.0-T MR Imaging and Gleason Grade in Peripheral Zone Prostate Cancer. Radiology. 2011;259(2):453–461. doi:10.1148/radiol.11091409. [PubMed: 21502392]

[25]. Li L, Margolis DJ, Deng M, Cai J, Yuan L, Feng Z, Min X, Hu Z, Hu D, Liu J and Wang L Correlation of gleason scores with magnetic resonance diffusion tensor imaging in peripheral zone prostate cancer. J Magn Reson Imaging. 2015;42(2):460–467. doi:10.1002/jmri.24813. [PubMed: 25469909]

[26]. Noworolski SM, Vigneron DB, Chen AP, Kurhanewicz J. Dynamic Contrast-Enhanced MRI and MR Diffusion to Distinguish Between Glandular and Stromal Prostatic Tissues. Magn Reson Imaging. 2008;26(8):1071–1080. doi:10.1016/j.mri.2008.01.033. [PubMed: 18508221]

Author Manuscript Author Manuscript Author Manuscript Author Manuscript

[27]. Vos EK, Litjens GJ, Kobus T, et al. Assessment of prostate cancer aggressiveness using dynamic contrast-enhanced magnetic resonance imaging at 3 T. Eur Urol. 2013;64(3):448–455. doi:10.1016/j.eururo.2013.05.045. [PubMed: 23751135]

[28]. Kobus T, Hambrock T, Hulsbergen-van de Kaa CA, et al. In vivo assessment of prostate cancer aggressiveness using magnetic resonance spectroscopic imaging at 3 T with an endorectal coil. Eur Urol. 2011;60(5):1074–1080. doi:10.1016/j.eururo.2011.03.002. [PubMed: 21419565]

[29]. Bourne RM, Kurniawan N, Cowin G, Sved P, Watson G. Microscopic diffusion anisotropy in formalin fixed prostate tissue: preliminary findings. Magn Reson Med. 2012;68(6):1943–1948. doi:10.1002/mrm.24179. [PubMed: 22287422]

[30]. Kitzing YX, Prando A, Varol C, Karczmar GS, Maclean F, Oto A. Benign Conditions That Mimic Prostate Carcinoma: MR Imaging Features with Histopathologic Correlation. RadioGraphics. 2016;36:162–175. doi:10.1148/rg.2016150030. [PubMed: 26587887]

[31]. Kurhanewicz J, Vigneron DB, Nelson SJ, Hricak H, MacDonald JM, Konety B, Narayan P. Citrate as an in vivo marker to discriminate prostate cancer from benign prostatic hyperplasia and normal prostate peripheral zone: detection via localized proton spectroscopy. Urology. 1995 Mar;45(3):459–66. doi:10.1016/S0090-4295(99)80016-8. [PubMed: 7533458]

[32]. Roehrborn CG. Pathology of benign prostatic hyperplasia. Int J Impot Res. 2008;20;S11–S18. doi:10.1038/ijir.2008.55.

[33]. Tosoian JJ, Alam R, Ball MW, Carter HB, Epstein JI. Managing high-grade prostatic intraepithelial neoplasia (HGPIN) and atypical glands on prostate biopsy. Nat Rev Urol. 2018;15;55–66. doi:10.1038/nrurol.2017.134. [PubMed: 28858331]

[34]. Peng YH, Jiang YL, Yang C, et al. Quantitative Analysis of Multiparametric Prostate MR Images: Differentiation between Prostate Cancer and Normal Tissue and Correlation with Gleason Score-A Computer-aided Diagnosis Development Study. Radiology. 2013;267(3):787–796. doi:10.1148/radiol.13121454. [PubMed: 23392430]

[35]. Vos EK, Kobus T, Litjens GJ, et al. Multiparametric Magnetic Resonance Imaging for Discriminating Low-Grade From High-Grade Prostate Cancer. Invest Radiol. 2015;50(8):490–497. doi:10.1097/RLI.0000000000000157. [PubMed: 25867656]

[36]. Fehr D, Veeraraghavan H, Wibmer A, et al. Automatic classification of prostate cancer Gleason scores from multiparametric magnetic resonance images. Proc Natl Acad Sci USA. 2015;112(46):E6265–6273. https://doi.org/ [PubMed: 26578786]

[37]. Dikaios N, Alkalbani J, Sidhu HS, et al. Logistic regression model for diagnosis of transition zone prostate cancer on multi-parametric MRI. Eur Radiol. 2015;25(2):523–532. doi:10.1073/pnas.1505935112. [PubMed: 25226842]

[38]. Hambrock T, Vos PC, Hulsbergen-van de Kaa CA, Barentsz JO, Huisman HJ. Prostate cancer: computer-aided diagnosis with multiparametric 3-T MR imaging--effect on observer performance. Radiology. 2013;266(2):521–530. doi:10.1148/radiol.12111634. [PubMed: 23204542]

[39]. Hoeks CM, Hambrock T, Yakar D, et al. Transition zone prostate cancer: detection and localization with 3-T multiparametric MR imaging. Radiology. 2013;266(1):207–217. doi:10.1148/radiol.12120281. [PubMed: 23143029]

[40]. Ocak I, Bernardo M, Metzger G, Barrett T, Pinto P, Albert PS, Choyke PL. Dynamic Contrast-Enhanced MRI of Prostate Cancer at 3 T: A Study of Pharmacokinetic Parameters. AJR Am J Roentgenol. 2007;189:W192–W201. doi:10.2214/AJR.06.1329.

[41]. Gupta RT, Kauffman CR, Garcia-Reyes K, Palmeri ML, Madden JF, Polascik TJ, Rosenkranz AB. Apparent Diffusion Coefficient Values of the Benign Central Zone of the Prostate: Comparison With Low- and High-Grade Prostate Cancer. AJR Am J Roentgenol. 2015;205:331–336. doi:10.2214/AJR.14.14221. [PubMed: 26204283]

[42]. Chesnais AL, Niaf E, Bratan F, Mege-Lechevallier F, Roche S, Rabilloud M, Colombel M, Rouviere O. Differentiation of transitional zone prostate cancer from benign hyperplasia nodules: Evaluation of discriminant criteria at multiparametric MRI. Clin Radiol. 2013;68:e323–e330. doi:10.1016/j.crad.2013.01.018. [PubMed: 23528164]

[43]. Elbuluk O, Muradyan N, Shih J, et al. Differentiating Transition Zone Cancers From Benign Prostatic Hyperplasia by Quantitative Multiparametric Magnetic Resonance Imaging.

Author Manuscript Author Manuscript Author Manuscript Author Manuscript

J Comput Assist Tomogr. 2016;40(2):218–224. doi:10.1097/RCT.0000000000000353. [PubMed: 26760185]

[44]. Dwivedi DK, Kumar R, Bora GS, Sharma S, Thulkar S, Gupta SD, Jagannathan NR. Multiparametric MR can identify high grade prostatic intraepithelial neoplasia (HGPIN) lesions and predict future detection of prostate cancer in men with a negative initial prostate biopsy. Magn Reson Imaging. 2016;34:1081–1086. doi:10.1016/j.mri.2016.05.006. [PubMed: 27211254]

[45]. Sciarra A, Panebianco V, Ciccariello M, Salciccia S, Lisi D, Osimani M, Alfarone A, Gentilucci A, Parente U, Passariello R, Gentile V. Magnetic Resonance Spectroscopic Imaging (1H-MRSI) and Dynamic Contrast-Enhanced Magnetic Resonance (DCE-MRI): Pattern Changes From Inflammation to Prostate Cancer. Cancer Invest. 2010;28(4):424–432. doi:10.1080/07357900903287048. [PubMed: 20073578]

[46]. Litjens GJS, Elliott R, Shihc N, Feldmanc M, Barentsza JO, Hulsbergen - van de Kaaa CA, Kovacsa I, Huismana HJ, Madabhushib A. Distinguishing prostate cancer from benign confounders via a cascaded classifier on multi-parametric MRI. Med Imaging - Proc SPIE. 2014;9035:903512. doi:10.1117/12.2043751.

[47]. Litjens GJ, Elliott R, Shih NN, et al. Computer-extracted Features Can Distinguish Noncancerous Confounding Disease from Prostatic Adenocarcinoma at Multiparametric MR Imaging. Radiology. 2016;278(1):135–145. doi:10.1148/radiol.2015142856. [PubMed: 26192734]

[48]. Giganti F, Kasivisvanathan V, Kirkham A, Punwani S, Emberton M, Moore CM, et al. Prostate MRI quality: a critical review of the last 5 years and the role of the PI-QUAL score. Br J Radiol 2021;94:20210415. doi:10.1259/bjr.20210415.

Author Manuscript Author Manuscript Author Manuscript Author Manuscript

- We differentiated tissues of the prostate by comparing mpMRI and histopathology.
- mpMRI parameters were characterized separately per zone and by tissue type.
- Logistic regression model fits differentiated cancer from benign tissues.
- Model fits achieved ROC AUCs ≥ 0.91.

Author Manuscript Author Manuscript Author Manuscript Author Manuscript

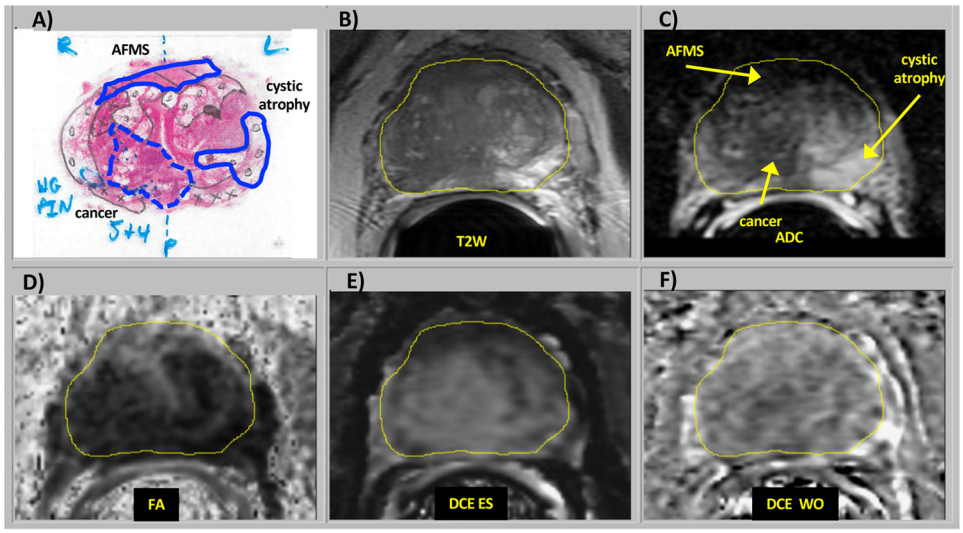

Figure 1:

Images from a 65 year-old male with serum PSA of 9.54ng/ml and GS5+4 prostate cancer who underwent radical prostatectomy. a) H&E stained histology specimen, b) coil-corrected T2-weighted FSE image, c) ADC map, d) fractional anisotropy map, e) maximal enhancement slope, f) washout slope. ROIs of cancer (dashed outline), AFMS (slashes), and cystic atrophy (circles) are highlighted in the histology and ADC images.

Author Manuscript Author Manuscript Author Manuscript Author Manuscript

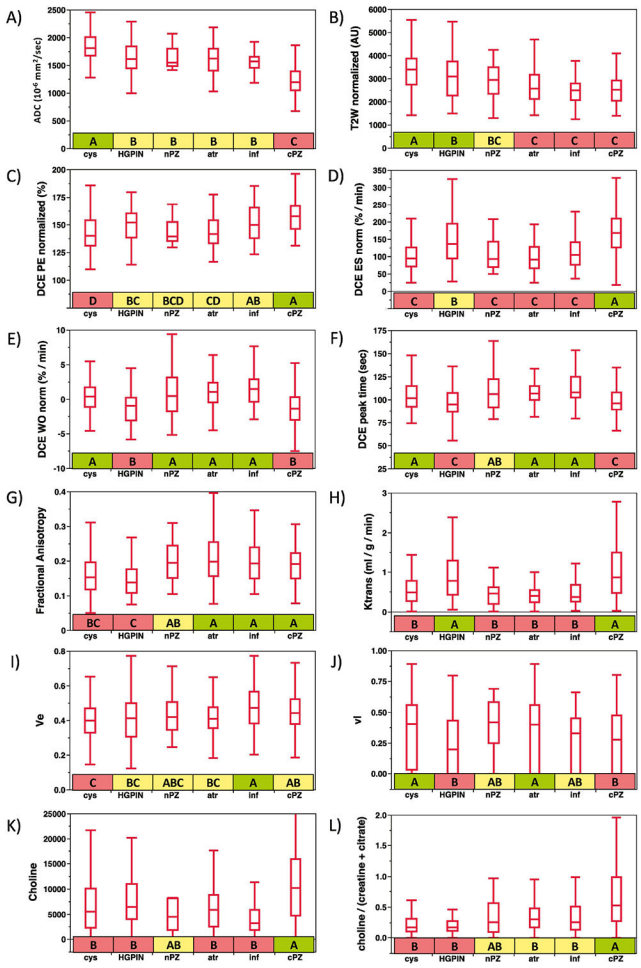

Figure 2:

Box-plots comparing MR parameters in peripheral zone tissues A) ADC, B) T2-weighted intensity, C) DCE MRI Peak Enhancement, D) DCE MRI Enhancement Slope, E) DCE MRI Washout Slope F) DCE MRI Peak Time, G) K^{trans}, H) v_E, I) v_L, J) Choline, K) Choline/(Creatine + Citrate). Letter labels (A, B, C, D) within each plot indicate means that are significantly different by p-value < 0.05, whereas multiple letter labels for a group indicate that group is not significantly different from groups with the same labels. Colors highlight high, middle, and low parameters.

Author Manuscript Author Manuscript Author Manuscript Author Manuscript

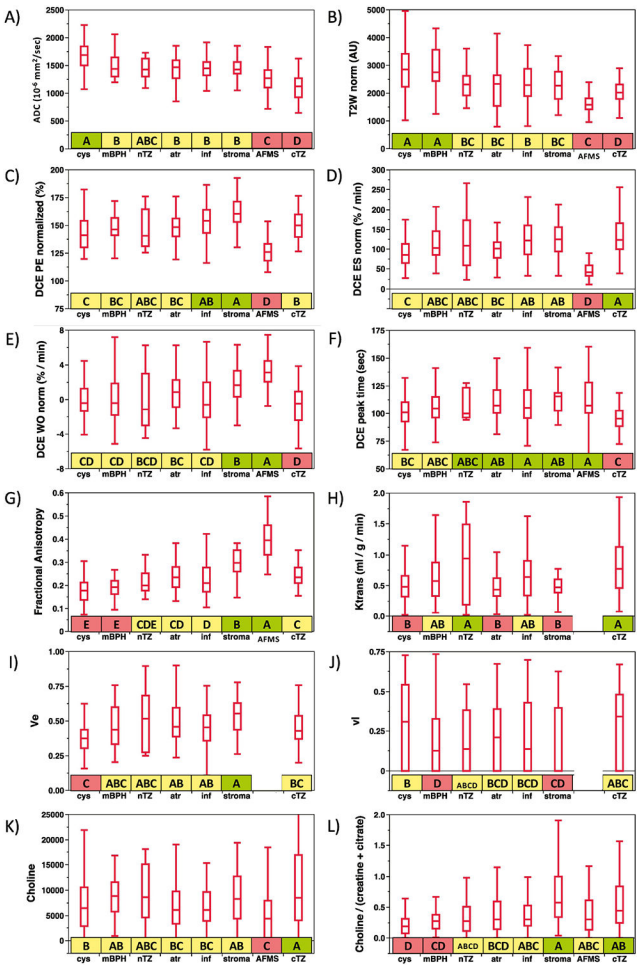

Figure 3:

Box-plots comparing MR parameters in transition zone tissues A) ADC, B) T2-weighted intensity, C) DCE MRI Peak Enhancement, D) DCE MRI Enhancement Slope, E) DCE MRI Washout Slope, F) DCE MRI Peak Time, G) K^{trans}, H) v_{EES}, I) v_L, J) Choline, K) Choline/(Creatine + Citrate). Letter labels (A, B, C, D) within each plot indicate means that are significantly different by p-value < 0.05, whereas multiple letter labels for a group indicate that group is not significantly different from groups with the same labels. Colors highlight high, middle, and low parameters.

Author Manuscript Author Manuscript Author Manuscript Author Manuscript

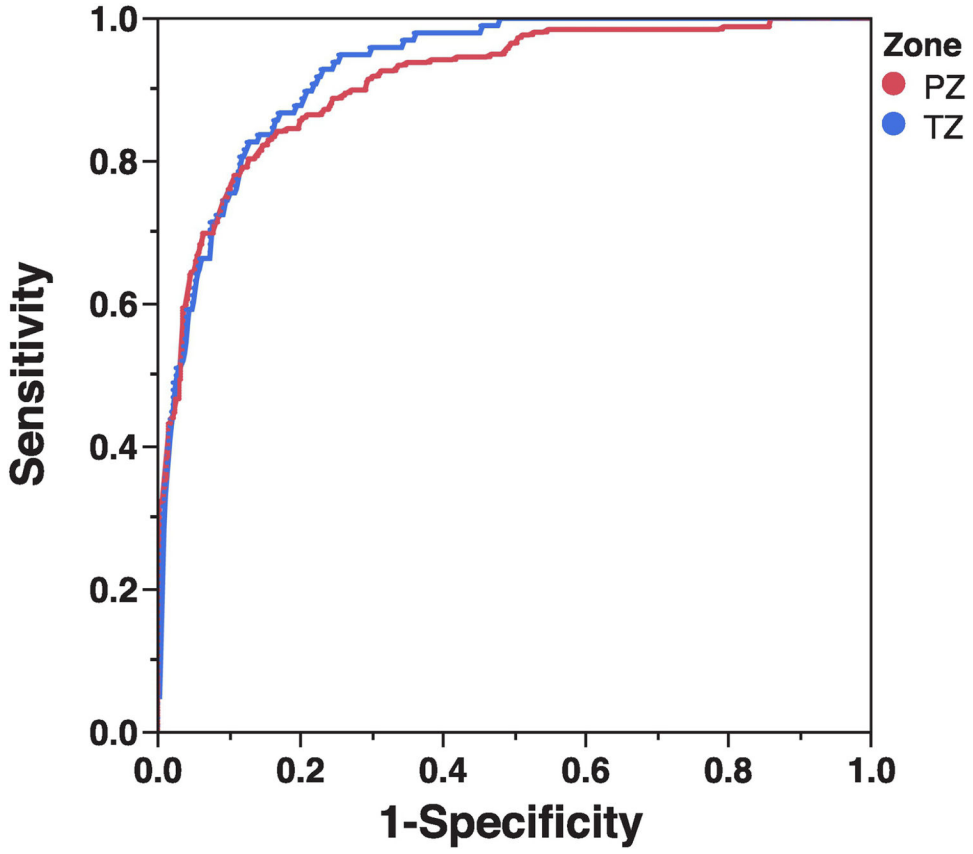

Figure 4:
ROC curves from the logistic regression fits of PCa vs benign tissues for the PZ (red) and the TZ (blue).

Author Manuscript Author Manuscript Author Manuscript Author Manuscript

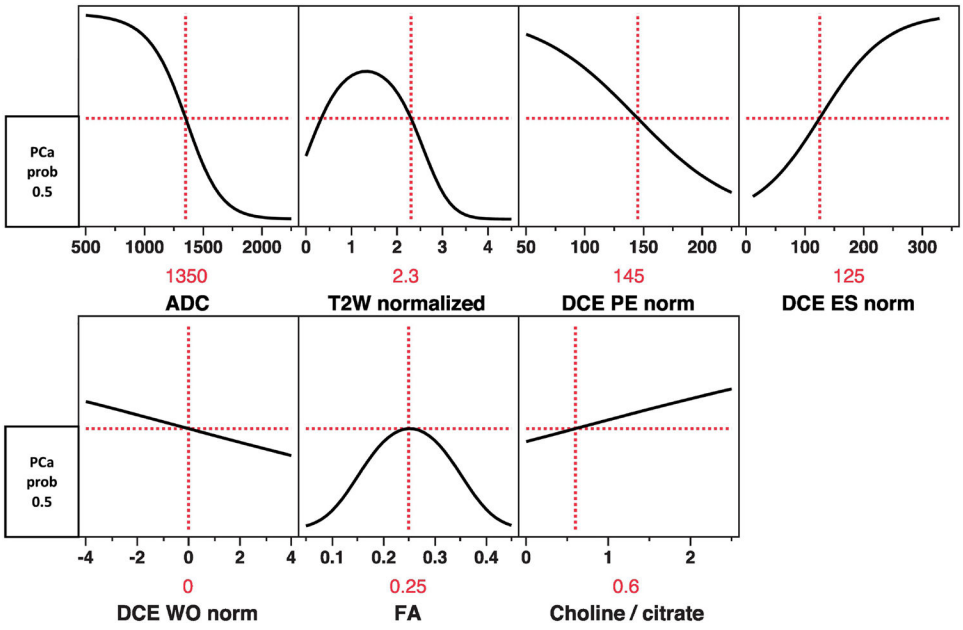

Figure 5:
Profiler plots with cursors set for parameters between PCa and benign for the TZ model.

Author Manuscript Author Manuscript Author Manuscript Author Manuscript

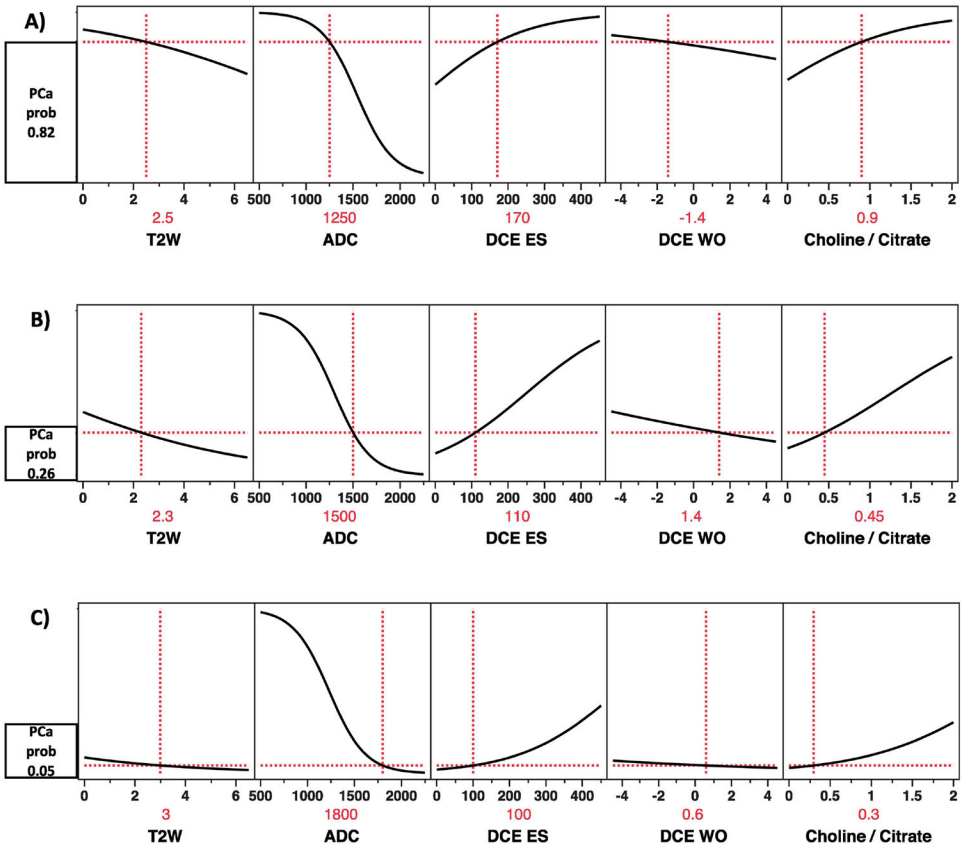

Figure 6:
Profiler plots for the PZ model with cursors set for parameters to compare a) PCa, b) inflammation and b) cystic atrophy.

Author Manuscript

Author Manuscript

Author Manuscript

Author Manuscript

Table 1:

Tissue region of interest (ROI) counts and sizes.

Prostate Region	Tissue Type	Number of patients	Number of patients (tissue group)	Number of ROIs	Number of ROIs (tissue group)	ROI size (cc) Median (Q1, Q3)
Transition Zone	cys	36	42	138	193	0.10 (0.07, 0.16)
	mBPH	13		55		0.19 (0.13, 0.27)
	nTZ	9	9	13	13	0.16 (0.10, 0.23)
	inf	31	41	114	168	0.07 (0.04, 0.11)
	atr	24		54		0.13 (0.09, 0.22)
	stroma	20	20	47	47	0.25 (0.17, 0.36)
	AFMS	42	42	94	94	0.21 (0.13, 0.29)
	cTZ	22	22	102	102	0.13 (0.09, 0.20)
	Total				617	0.12 (0.08, 0.22)
Peripheral Zone	cys	56	61	189	295	0.11 (0.07, 0.16)
	HGPIN	32		106		0.11 (0.08, 0.16)
	nPZ	22	22	25	25	0.07 (0.05, 0.10)
	atr	38	58	133	215	0.12 (0.08, 0.18)
	inf	30		82		0.07 (0.05, 0.11)
	cPZ	57	57	276	276	0.13 (0.08, 0.20)
	Total				811	0.11 (0.07, 0.16)

Data reported as median (first quartile (Q1), third quartile (Q3)).

Cys = cystic atrophy, mBPH = mixed BPH, nTZ = normal TZ, inf = inflammation, atr = atrophy, AFMS = anterior fibromuscular stroma, cTZ = cancerous TZ

Author Manuscript Author Manuscript Author Manuscript Author Manuscript

Table 2:

Parameter values for peripheral zone tissues

	Group	Tissue	ADC (10^{-6} mm^2/sec)	T2W_norm (AU)	DCE MRI PE norm (%)	DCE MRI ES norm (% / min)	DCE MRI WO norm (% / min)	DCE MRI pktime (sec)	FA
More ↑	2	Cys	1800 ± 240	3.3 ± 0.11	43 ± 16	100 ± 43	0.58 ± 2.7	100 ± 28	0.16 ± 0.06
		HGPIN	1600 ± 260	3.0 ± 0.11	50 ± 15	150 ± 67	-1.3 ± 2.4	100 ± 17	0.16 ± 0.07
		nPZ	1650 ± 200	2.7 ± 0.76	46 + 14	100 ± 43	0.96 ± 3.7	110 ± 35	0.20 ± 0.05
	1	atr	1600 ± 270	2.7 ± 0.92	44 + 15	100 ± 52	1.2 ± 2.9	110 ± 26	0.21 ± 0.08
Less Glandular		infl	1500 ± 210	2.3 ± 0.62	51 + 16	110 ± 54	1.4 ± 2.8	120 ± 23	0.21 ± 0.09
		cPZ	1200 ± 260	2.5 ± 0.74	57 + 15	170 ± 65	-1.3 ± 3.1	100 ± 27	0.19 ± 0.06

	Group	Tissue	K^{trans} (ml/g/min)	v_{EES}	v_L	Choline (AU)	Choline / Citrate
More ↑	2	Cys	0.6 ± 0.36	0.41 ± 0.15	0.35 ± 0.25	7 ± 10	0.3 ± 0.27
		HGPIN	1.0 ± 0.87	0.41 ± 0.13	0.25 ± 0.25	9 ± 7	0.3 ± 0.24
		nPZ	0.5 ± 0.37	0.43 ± 0.12	0.39 ± 0.22	7 ± 7	0.4 ± 0.33
	1	atr	0.4 ± 0.27	0.43 ± 0.13	0.34 ± 0.25	6 ± 5	0.5 ± 0.36
Less Glandular		infl	0.5 ± 0.35	0.50 ± 0.15	0.28 ± 0.21	5 ± 4	0.5 ± 0.32
		cPZ	1.2 ± 0.98	0.45 ± 0.12	0.26 ± 0.23	12 ± 16	0.9 ± 0.73

Cys = cystic atrophy, HGPIN = high grade PIN, nPZ = normal PZ, atr = atrophy, inf = inflammation, cPZ = cancerous PZ

Author Manuscript

Author Manuscript

Author Manuscript

Author Manuscript

Table 3:

Parameter values for transition zone tissues

	Group	Tissue	ADC (10^{-3} mm^2/sec)	T2W_norm (AU)	DCE MRIpe_norm (%)	DCE MRIes_norm (% / min)	DCE MRIwo_norm (% / min)	DCE MRIpktime (sec)	FA
More ↑	2	Cys	1.6 ± 0.29	2.7 ± 0.83	43 ± 15	100 ± 50	-0.2 ± 1.9	100 ± 20	0.18 ± 0.06
		mBPH	1.5 ± 0.22	2.9 ± 0.88	50 ± 14	120 ± 51	0.0 ± 2.5	100 ± 25	0.19 ± 0.04
	1	nTZ	1.5 ± 0.20	2.3 ± 0.64	47 ± 18	120 ± 69	0.0 ± 3.6	120 ± 36	0.21 ± 0.05
		Infl	1.4 ± 0.18	2.2 ± 0.79	53 ± 14	130 ± 53	0.1 ± 3.0	110 ± 32	0.22 ± 0.07
		Atr	1.5 ± 0.22	2.2 ± 0.93	49 ± 14	110 ± 45	1.0 ± 2.5	110 ± 23	0.24 ± 0.07
Less ↓		stroma	1.5 ± 0.18	2.2 ± 0.73	60 ± 18	130 ± 42	1.6 ± 2.3	110 ± 12	0.30 ± 0.06
Glandular		AFMS	1.3 ± 0.23	1.6 ± 0.39	28 ± 14	50 ± 22	3.4 ± 2.0	110 ± 24	0.40 ± 0.08
		cTZ	1.1 ± 0.24	1.9 ± 0.53	50 ± 12	140 ± 47	-0.8 ± 2.6	100 ± 30	0.25 ± 0.07

	Group	Tissue	Ktrans (ml/g/min)	V_{EES}	v_L	Choline	Choline / Citrate
More ↑	2	Cys	0.56 ± 0.43	0.40 ± 0.13	0.29 ± 0.25	7.9 ± 7.1	0.34 ± 0.25
		mBPH	0.70 ± 0.50	0.46 ± 0.15	0.17 ± 0.19	9.2 ± 4.4	0.43 ± 0.24
	1	nTZ	0.76 ± 0.66	0.52 ± 0.23	0.19 ± 0.20	9.3 ± 5.9	0.59 ± 0.45
		Infl	0.70 ± 0.46	0.47 ± 0.16	0.21 ± 0.22	7.3 ± 5.3	0.54 ± 0.39
		Atr	0.53 ± 0.37	0.48 ± 0.15	0.21 ± 0.21	8.0 ± 7.8	0.41 ± 0.33
Less ↓		Stroma	0.53 ± 0.31	0.54 ± 0.13	0.17 ± 0.21	8.7 ± 4.9	0.54 ± 0.33
Glandular		AFMS	0.20 ± 0.18	0.54 ± 0.21	0.39 ± 0.24	5.1 ± 4.6	0.40 ± 0.26
		cTZ	0.88 ± 0.56	0.45 ± 0.13	0.29 ± 0.23	11.7 ± 8.6	0.70 ± 0.55

Cys = cystic atrophy, mBPH = mixed BPH, nTZ = normal TZ, inf = inflammation, atr = atrophy, AFMS = anterior fibromuscular stroma, cTZ = cancerous TZ

Author Manuscript

Author Manuscript

Author Manuscript

Author Manuscript

Table 4:

Comparison of parameters in PZ vs TZ

Parameter	cystic atrophy		normal		atrophy		inflammation	
	ratio	p-value	ratio	p-value	ratio	p-value	ratio	p-value
ADC	1.11	< **0.01**	1.13	< **0.01**	1.11	< **0.01**	1.09	< **0.01**
T2W	1.20	< **0.01**	1.26	**0.01**	1.26	< **0.01**	1.06	0.14
DCE MRI washout *	0.73	< **0.01**	0.93	0.46	0.24	0.58	1.10	< **0.01**
FA	0.92	**0.03**	0.95	0.54	0.87	< **0.01**	0.93	0.17
vL	1.17	0.07	1.99	0.01	1.57	< **0.01**	1.41	< **0.01**
creatine	0.82	**0.04**	0.73	0.34	0.75	**0.04**	0.74	**0.02**

* DCE MRI washout = DCE MRI washout in PZ – TZ; remaining values are ratios of PZ/TZ mean measures.

Author Manuscript

Author Manuscript

Author Manuscript

Author Manuscript

Table 5:

Area under the curve (AUC) and confidence intervals (CI) from training and validation models using repeated 4-fold cross validation.

Model	Transition Zone			Peripheral Zone		
	AUC	**sens**	**spec**	**AUC**	**sens**	**spec**
Total	0.93	0.83	0.86	0.91	0.83	0.85
	AUC	**95% CI**		**AUC**	**95% CI**	
Training	0.93	0.92	0.94	0.91	0.91	0.92
Validation	0.93	0.90	0.95	0.91	0.89	0.93